### ORIGINAL ARTICLE



Check for updates

# Differences in indentation and wear behaviors between the two sides of thermally tempered soda lime silica glass

Hongtu He<sup>1,2</sup> | Hongshen Liu<sup>2</sup> | Yen-Ting Lin<sup>2</sup> | Conghang Qu<sup>3</sup> | Jiaxin Yu<sup>1</sup> | Seong H. Kim<sup>2,3</sup> |

<sup>1</sup>Key Laboratory of Testing Technology for Manufacturing Process, Ministry of Education, Southwest University of Science and Technology, Mianyang, Sichuan, China

<sup>2</sup>Department of Chemical Engineering and Materials Research Institute, Pennsylvania State University, State College, PA, USA

<sup>3</sup>Department of Materials Science and Engineering, Pennsylvania State University, State College, PA, USA

#### Correspondence

Hongtu He, Key Laboratory of Testing Technology for Manufacturing Process, Ministry of Education, Southwest University of Science and Technology, Mianyang 621010, Sichuan, China. Email: hehongtu@swust.edu.cn

Seong H. Kim, Department of Chemical Engineering and Materials Research Institute, Pennsylvania State University, State College, PA 16802, USA. Email: shkim@engr.psu.edu

## **Funding information**

National Natural Science Foundation of China, Grant/Award Number: 51605401; National Science Foundation, Grant/ Award Number: DMR-2011410

#### **Abstract**

Thermal tempering is an industrial process widely used to make soda lime silica (SLS) glass panels stronger and tougher. During the tempering process, the upper and bottom sides of the glass may experience different cooling rates, and thus, their properties could be different. This study characterized changes in surface composition and subsurface glass network structures as well as indentation and wear resistance properties of the air- and tin-sides of 6-mm-thick SLS window panels faced toward the upper and sliding roller sides during thermal tempering. The results showed that although the chemical and structural differences detected with X-ray photoelectron spectroscopy and specular reflection infrared spectroscopy are subtle, there are large differences in nanoindentation behaviors and mechanochemical wear properties of the SLS glass surface. The findings of this study provide further insights into the performance difference between the air- and tin-sides of the SLS glass panel treated with thermal tempering.

### KEYWORDS

nanoindentation, soda lime silica, tempered glass, Vickers indentation, wear resistance

# 1 | INTRODUCTION

Soda lime silica (SLS) glass is a commodity product widely used in architecture, transportation, and energy industries due to its high optical transparency and good mechanical and chemical durability as well as its processibility for mass production. <sup>1-3</sup> Due to the higher mechanical strength of tempered glass compared to the annealed glass, the tempered SLS glass can meet higher safety requirements for structural element applications. <sup>4,5</sup> During the manufacturing

and application process,SLS glass surfaces are physically contacted with foreign objects and under harsh conditions, they could be damaged due to indentation or frictional stress during contacts.<sup>6,7</sup> Such physical damages will not only lead to optical scattering but also reduce the mechanical and chemical durability of the glass object.<sup>8,9</sup> Thus, understanding fundamental mechanical properties and their dependence on manufacturing process is important to prevent the surface damage of SLS glass under various normal and tangential stress conditions.

Mechanical responses of SLS glass under a stress along the surface normal direction include elastic deformation (reversible recovery during the removal of applied load), densification (subsurface structural change due to compression, which can be recovered upon annealing), plastic or shear flow (leaving permanent change in surface topography), and cracking. <sup>10–12</sup> These indentation behaviors can be further affected by the indenter geometry, <sup>13</sup> the loading rate, <sup>14</sup> and the glass composition. <sup>15</sup> For instance, increasing the sharpness of the indenter tip can cause more shear deformation or cracking and less densification, and increasing the loading rate can result in less shear deformation of SLS glass. <sup>13,14</sup> The indentation damage of SLS glass surface can be improved by surface treatments such as ion-exchange <sup>16</sup> and aging or soaking. <sup>17</sup>

The wear behavior of SLS glass is sensitive to the humidity of ambient air. 18 In reciprocating scratch (wear) tests with smooth counter-surfaces, it was found that the wear of SLS glass peculiarly decreased at near-saturation RH, while the wear of fused quartz, borosilicate, and aluminosilicate glasses increased as RH increased. 19,20 The increase in wear with RH could be explained with the classical stress-corrosion theory in which the adsorbed water molecules are thought to facilitate the hydrolysis of Si-O-Si network under mechanical stress. 11 However, this theory cannot explain the enhanced resistance of SLS against wear at high RH. Further studies suggested this unusual wear behavior of SLS glass in humid air could be attributed to the presence of leachable sodium ions (Na<sup>+</sup>) and the water activity on the glass surface.<sup>21–24</sup> Since the glass wear in humid air involves chemical reactions of water molecules adsorbed on the glass surface, 25-27 it is usually called "mechanochemical" wear and should be differentiated from 'mechanical' wear (or abrasive scratch) occurring in dry condition. The wear behavior of SLS glass can be further affected by the sliding speed<sup>28</sup> and the countersurface chemistry. 25,29

The mechanical and mechanochemical properties of glass are a function of not only the bulk composition but also the thermal history of the sample. Previously, it was reported that the tempered SLS solar panel showed a higher hardness compared to the annealed panel, but it exhibited less scratch resistance and more chipping in a single scratch test. 4,30 In another study with reciprocating wear tests, no significant difference was found between the annealed and tempered SLS float glass when the wear tests were conducted in dry and low RH conditions (40% RH), but the mechanochemical wear behavior in high RH conditions (90% RH) was somewhat different between air- and tin-sides of annealed and tempered glass.<sup>31</sup> Although some of the advanced tempering furnaces are based on the air-flotation technique, most custom tempering furnaces still use the sliding roller conveyer mode.<sup>32</sup> During the tempering process of SLS float glass, the bottom side of the float glass is contacted with the roller conveyer,

while the opposite (upper) side does not have any physical contact.<sup>33</sup> The glass surface contacting with the sliding roller may experience different thermal history, due to different air flow conditions, compared to the opposite side of float glass. The performance difference between these two sides of the tempered SLS glass has not been investigated systematically.

This study shows how the mechanical and mechanochemical properties of the air- and tin-sides of SLS float glass are altered upon thermal tempering with facing the sliding roller (down) or upper side during the tempering process. The chemical and structural changes upon tempering were analyzed with X-ray photoelectron spectroscopy (XPS) and specular reflection infrared (SR-IR) spectroscopy. The mechanical properties of the SLS glass surfaces were compared using nanoindentation and Vickers indentation tests, and the wear properties of glass were compared with reciprocating ball-on-flat tribo-tests in dry, intermediate, and near-saturation RH conditions (0%, 40%, and 90%). The experimental results observed in this study provide deeper insights needed for technological quality control during its manufacturing and application process of SLS glass panels.

### 2 | EXPERIMENTAL METHODS

SLS float glass panels with a 6-mm thickness were used in this study. The glass samples were thermally tempered using an industrial grade tempering facility (Oldcastle Building Envelope). The tempering process consisted of heating the panel to a temperature above the glass transition temperature followed by fast cooling with a high-speed air stream to room temperature, as illustrated in Figure 1A. To differentiate two sides of the tempered glass, the upper sides without contacting the conveyer and the bottom sides contacted with the sliding roller were referred as "T/up" and "T/roller", respectively, hereafter. In this study, one set of samples was prepared with the air-side of SLS float glass as the "T/up" configuration, while the other set was prepared with the air-side surface in the "T/roller" condition. As a reference sample, the annealed glass (AN) samples were prepared by heating the float glass manufactured from the same batch to the stress-relief point in the same furnace and then slowly cooling to room temperature (Figure 1A). Figure 1B compares the optical microscopy image of the fractured surface of each sample. The compressive surface layer appeared to be slightly thicker in the T/roller side than the T/up side.<sup>34</sup> This could mean that the compressive stress casing might be slightly thicker in the T/roller side, although both sides were treated in the same tempering process. Prior to the surface characterization, glass samples were cleaned by rinsing with deionized water, ethanol, and deionized water again and then blow drying with nitrogen followed by UV-ozone cleaning to remove organic contaminants.<sup>19</sup>

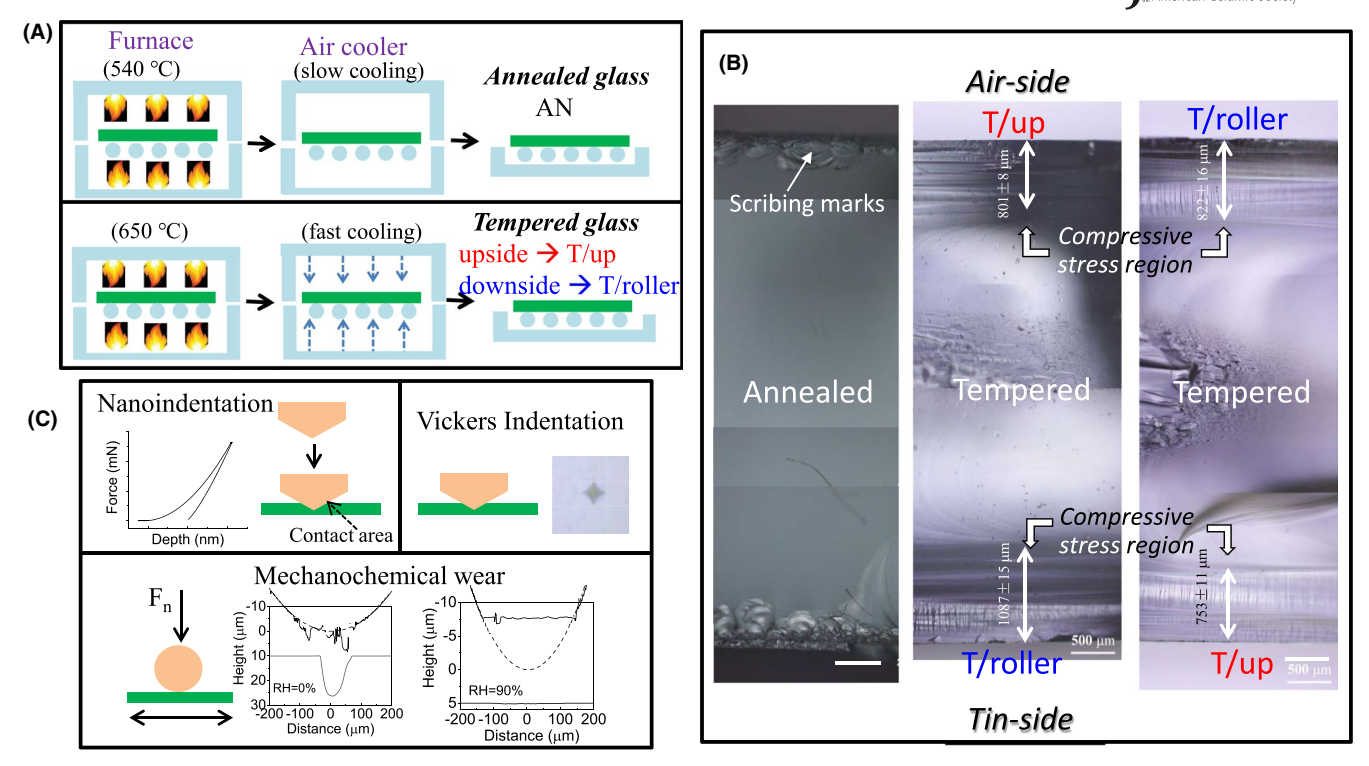


FIGURE 1 (A) Sample preparation of annealed glass and tempered glass. (B) Optical microscopy images of the fractured surfaces of annealed and tempered glass. Note that more than five images are taken at the selected location of a given sample, and those images are stitched to show the full view across the fractured glass surface. At the location where the stress intensity factor at the propagating crack front drops below the fracture toughness, the Wallner lines (not clear in optical image) become parallel to the external surface; the compressive stress gradient exists from that location to the external surface (marked with white double arrows). The averaged value and standard error of mean (SEM) of the thickness of compressive stress region are obtained from five individual samples. (C) Methods of mechanical and mechanochemical characterization of glass surface

XPS analysis was performed using a PHI VersaProbe system equipped with an Al-K $\alpha$  x-ray source and a charge neutralizer (Chanhassen, MN). Low-resolution scans with a 117-eV pass energy were performed over narrow binding energy ranges of the O 1s, Na KLL, Sn 3d, Ca 2p, Mg KLL, K 2p, C 1s, Si 2p, and Al 2p components. A high-resolution scan of the C 1s region was collected with a 29-eV pass energy. The relative atomic concentrations obtained from XPS spectra were corrected for adventitious carbon contamination on the glass surface. The relative atomic concentrations of bridging oxygen (BO), nonbridging oxygen (NBO), and silanol (OH) groups were calculated using a stoichiometry-based structural model. The More details about the XPS experiments and the calculation of relative atomic concentration can be found in our previous publications. The structural model of the calculation of relative atomic concentration can be found in our previous publications.

SR-IR analysis was performed using a Bruker Hyperion 3000 microscope (Bruker Optics GmbH, Ettlingen, Germany). The spectra were collected with a 15× objective at a 20° incident angle over a 140 × 140  $\mu$ m<sup>2</sup> area and were acquired by averaging 400 scans at a 4 cm<sup>-1</sup> step size. A clean gold film was used as a reference for the IR power correction.

Nanoindentation tests was carried out with a Hysitron TI 950 triboindenter (Minneapolis, MN) with a Berkovich tip

in ambient air with ~44% RH. The maximum indentation force was varied from 4 to 8 mN with a 0.5-mN increment. The indentation was done following the standard procedure: 5 s for loading with a linear increase of indentation force to the maximum preset value, 2 s for holding at the maximum force, and then 5 s for unloading to zero force. The reduced (elastic) modulus and nanohardness were calculated from the force-displacement (P-h) curves using the widely-accepted Oliver-Pharr model.<sup>37</sup> The average and standard deviation were obtained from 20 measurements for each sample, and three samples were analyzed to obtain reasonable statistics. Microscale hardness was were measured using a microindenter (Leco MHT Series 200, St. Joseph, MI) with a Vickers tip at ~40% RH. The Vickers indentation tests were performed at 200 gf for 15-s holding time and 15-s unloading time, and then the indent was photographed and analyzed. The average and standard deviation were obtained from more than 10 measurements for each sample. All the nanoindentation and Vickers indentation tests were performed at room temperature (22  $\pm$  1°C).

The wear test was conducted using a custom-made environment-controlled ball-on-flat reciprocating tribometer at 0%, 40%, and 90% RH. The details of the instrument,

wear test, and cleaning procedure can be found in our previous publications. <sup>19,25</sup> The balls used for tribo-tests were a ~2.23-mm diameter sphere of sodium borosilicate (expansion coefficient 3.3 ppm/K, McMaster-Carr Products Inc.). The applied load was 0.2 N, which corresponded to a Maximum Hertzian contact pressure of ~380 MPa on the flat SLS surface (without wear). After the wear test, the wear track was analyzed with optical profilometry (Nexview 3D, Middlefield, CT) without cleaning the wear debris on both SLS glass and ball surfaces. The wear rate was calculated by dividing the wear volume of the track with the applied load and sliding distance per cycle. <sup>38</sup>

# 3 | RESULTS AND DISCUSSION

# 3.1 | Compositional and structural changes of SLS surface upon thermal tempering

Figure 2A,B plots the elemental compositions, determined by XPS, of the SLS air-side and tin-side, respectively, which were annealed (AN) and tempered facing upward (T/up) and downward (T/roller). Small amounts of Sn detected on the air-side must come from contaminations during sample handling or annealing in the industrial-grade furnace previously used for thermal tempering. It is noted that the Na concentration is lower for the AN surface than the T/up and T/roller surfaces. This must be due to more evaporation of sodium<sup>36,39</sup> during the slow cooling process of the AN surface, compared to the fast cooling with the forced air blow during the tempering process.

The measured elemental compositions were used to calculate the areal density of BO, NBO, and OH groups per nm<sup>2</sup> averaged over the top ~10 nm from the surface following the model published previously, 35,36 which are shown in Figure 2C,D. This model considers the connectivity and charge neutrality of the network. 35,36 The BO areal density appears to be slightly lower for the T/up surface of the air-side and the T/roller surface of the tin-side. The NBO concentration is highest for the T/up surface for both air- and tin-sides. In the air-side, the differences in NBO areal density among the AN, T/up, and T/roller surfaces are almost oppositely mirrored in the OH areal density; thus, the sum of NBO and OH is relatively constant. In the tin-side, the T/roller surface shows a significantly higher OH density than the AN and T/up surfaces. The source for this higher OH areal density for the T/ roller surface of the tin-side could not be identified in this study.

Figure 3 compares the SR-IR spectra of the Si–O stretch mode of the SLS glass. the broad band centered around 1050-1060 cm<sup>-1</sup> is assigned to the Si–O–Si (BO) stretch mode and the shoulder around 935 cm<sup>-1</sup> is assigned to the Si–O stretch mode of NBO and Si–OH.<sup>40,41</sup> Note that in this spectral range, the effective probe depth of SR-IR is ~2 μm for silicate glasses, <sup>42</sup> which is much thinner than the compressive stress casing produced by thermal tempering (typically ~20% of the sample thickness).<sup>31</sup> In the air-side, the thermal tempering does not appear to cause a large change in the network structure probed with SR-IR (Figure 3A). In the tin-side, the T/roller surface has noticeably larger shoulder at ~935 cm<sup>-1</sup> (Figure 3B). Although the effective probe depth is different and so it is difficult to make quantitative comparison, this

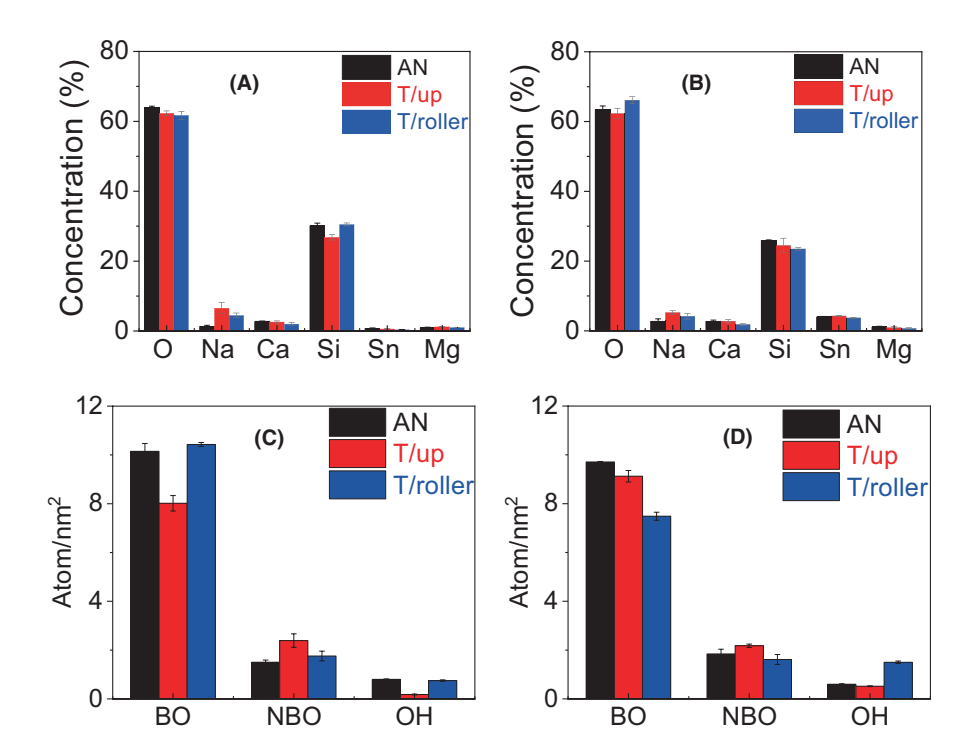
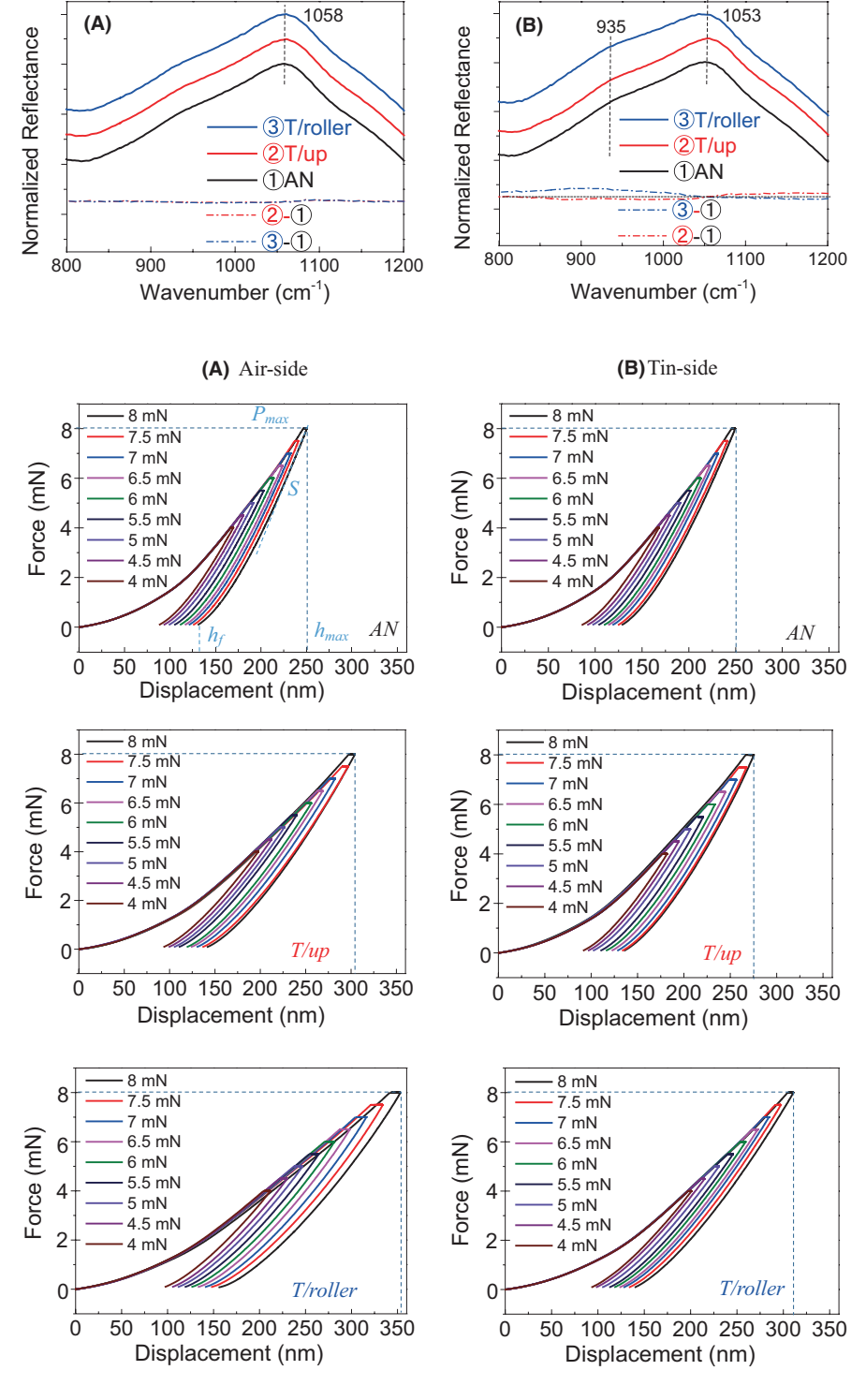


**FIGURE 2** (A, B) Surface composition and (C, D) oxygen speciation of (A, C) air-side and (B, D) tin-side of annealed and tempered SLS float glass. The error bar is the standard error of mean (SEM) from 3 measurements per sample. In (A, B), the difference in Na concentration between the AN surface versus T/up and T/roller surfaces is statistically significant (p < 0.05), while the difference between T/up vs. T/roller is statistically insignificant (p > 0.05)

FIGURE 3 SR-IR spectra of (A) air-side and (B) tin-side of annealed and tempered SLS glass. The dotted lines in the lower side are the difference between the tempered and annealed surface spectra

FIGURE 4 P-h curves of (A) airside and (B) tin-side of annealed and tempered SLS glass surfaces during the nanoindentation test. The maximum load  $(P_{\text{max}})$ , the maximum penetration depth  $(h_{\text{max}})$  during loading, the stiffness (S) upon elastic recovery at hmax during unloading, and the residual depth  $(h_f)$  at zero load are marked for  $P_{\text{max}} = 8$  mN in the top panel of (A); the same can be applied to all plots in other panels



might be relevant to the higher OH areal density determined in XPS analysis for this surface compared to the AN and T/up surfaces (Figure 2D).

# 3.2 | Changes in nanomechanical property of SLS surface upon thermal tempering

The mechanical properties of SLS surfaces at nanoscale were probed with nanoindentation. Figure 4 displays the

force-displacement (P-h) curves recorded during the loading, holding, and unloading cycles with various pre-set indentation forces. The most prominent effect noted in the P-h curves is that the maximum penetration depth  $(h_{\rm max})$  during the loading is drastically increased after thermal tempering which produces compressive stress in the surface region. This might be viewed counterintuitive because the surface with a compressive stress could be thought to have more resistance to indentation by a foreign object. But, the  $h_{\rm max}$  versus the maximum load  $(P_{\rm max})$  plot in Figure 5 clearly

indicates that the T/roller surface becomes more susceptible to the penetration at a given indentation load than the T/up surface, which is also more susceptible than the AN surface. Overall, the air-side becomes more penetrable than the tin-side after thermal tempering although the difference between these two is negligible for the annealed surfaces (Figure 5).

Although the tempered surfaces allow deeper penetration of the indenter during the loading process, they also have remarkably lager elastic recovery (quantified as  $1-h_f/h_{\rm max}$  in Figure 5) during unloading, compared to the annealed surface. In other words, the plastic deformation is significantly reduced for the tempered surfaces, compared to the annealed surface, although  $h_{\rm max}$  at a given  $P_{\rm max}$  is increased. This implies that the tempered surfaces can accommodate more strain energy through elastic processes than the annealed surface (see Figure S1). This must be associated with the toughening mechanism of the tempered glass with the compressive stress gradient in the surface region.  $^{31}$ 

The P-h curves shown in Figure 4 can be processed with the standard Oliver-Pharr model that is widely used to calculate the elastic modulus and hardness of materials. 43 For the tempered glass, the exact Poisson's ratio of the surface region with compressive stress is unknown<sup>4,30</sup>; thus, we use the reduced modulus, rather than elastic modulus here. Also, note that the Oliver-Pharr model is based on the projected area  $(A_c)$  calculated from a contact depth  $(h_c)$  which is estimated from  $h_{\text{max}}$ ,  $P_{\text{max}}$ , and stiffness (S) of the P-h curve (as marked in the top panel of Figure 4A as an example) assuming that the material is homogeneous and has no stress and its response is fully elastic; thus, it does not work well for the material with an internal stress gradient. 44-46 Then, the reduced modulus and hardness calculated from the P-h curves of the tempered surfaces must be taken as apparent values predicted from the Oliver-Pharr model assuming no internal stress, instead of true values which can be obtained only when the real contact area is known. The processed data are plotted in Figure 6.

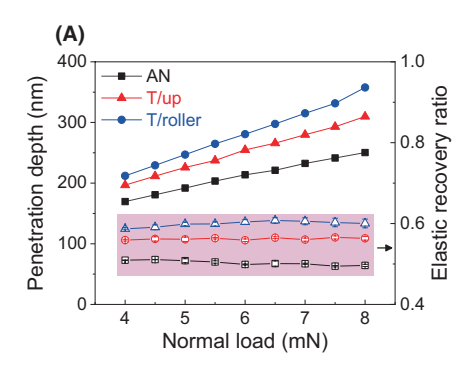
For the annealed glass, the reduced modulus and hardness calculated from the P-h curves (Figure 4) have negligible dependence on penetration depth (Figure 6) and agree well with the literature values for both air- and tin-sides of the SLS glass.  $^{47,48}$  In contrast, the *apparent* 

reduced modulus and apparent hardness of the tempered glass surface are significantly lower than those of the annealed glass. One may speculate that the pile-up around the nanoindentation may increase the contact area and thus reduce the calculated modulus and hardness. But when plastic deformation is small (i.e.,  $h_f/h_{\text{max}} < 0.7$ ), the Oliver-Pharr calculation is not significantly affected by the pile-up. <sup>49</sup> In Figure 6, the extent of reduction in the *appar*ent value from the corresponding AN value is larger for the T/roller surface than the T/up surface. This must be due to the difference in thermal history of these two surfaces during the thermal tempering process. The penetration depth dependence of the calculated apparent modulus and hardness values must be due to an artifact caused by ignoring the internal stress gradient of the tempered glass in the Oliver-Pharr model.

In Figure 4, it is noted that although  $h_{\rm max}$  is significantly larger for the tempered glass compared to the annealed glass at a given load,  $h_{\rm f}$  does not increase much. In a nanoscratch test with a conospherical tip at a ramp load up to 2.5 mN, the residual depth of the nanoscratch is found to be almost identical for the annealed and tempered glass surfaces (Figure S2). Thus, the real hardness (=  $P_{\rm max}$  ÷ residual imprint area) would have not been changed significantly.

# 3.3 | Changes in microhardness of SLS surface upon thermal tempering

In order to measure the hardness without the error of the standard Oliver-Pharr method, we have measured the hardness ( $H_V$ ) using the Vickers indentation method in which  $H_V$  is calculated by dividing the applied load with the *real* residual imprint area. Figure 7 shows the  $H_V$  values measured for the annealed and tempered SLS glass surfaces. For the air-side, the difference among the AN, T/up, and T/roller surfaces is statistically insignificant (p > 0.05, n = 11). For the tin-side, the difference of the T/roller surface from the AN and T/up surfaces appears to be statistically significant (p = 0.01, n = 11); however, the actual difference in magnitude is quite small. Thus, it can be concluded that the tempering process does not significantly alter the actual hardness of



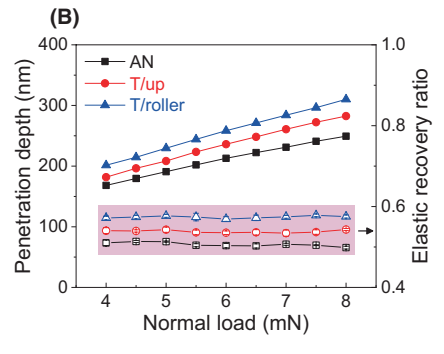


**FIGURE 5** Pentation depth  $(h_{\text{max}})$  during nanoindenation and elastic recovery ratio  $(1-h_f h_{\text{max}})$  of (A) air-side and (B) tin-side of the annealed and tempered SLS glass

FIGURE 6 (A, C) Reduced modulus and (B, D) hardness, calculated from the *P-H* curves shown in Figure 4 following the standard Oliver-Pharr model, for (A, B) air-side and (C, D) tin-side of annealed and tempered SLS glasses. The error bar is the standard error of mean from 20 measurements per sample

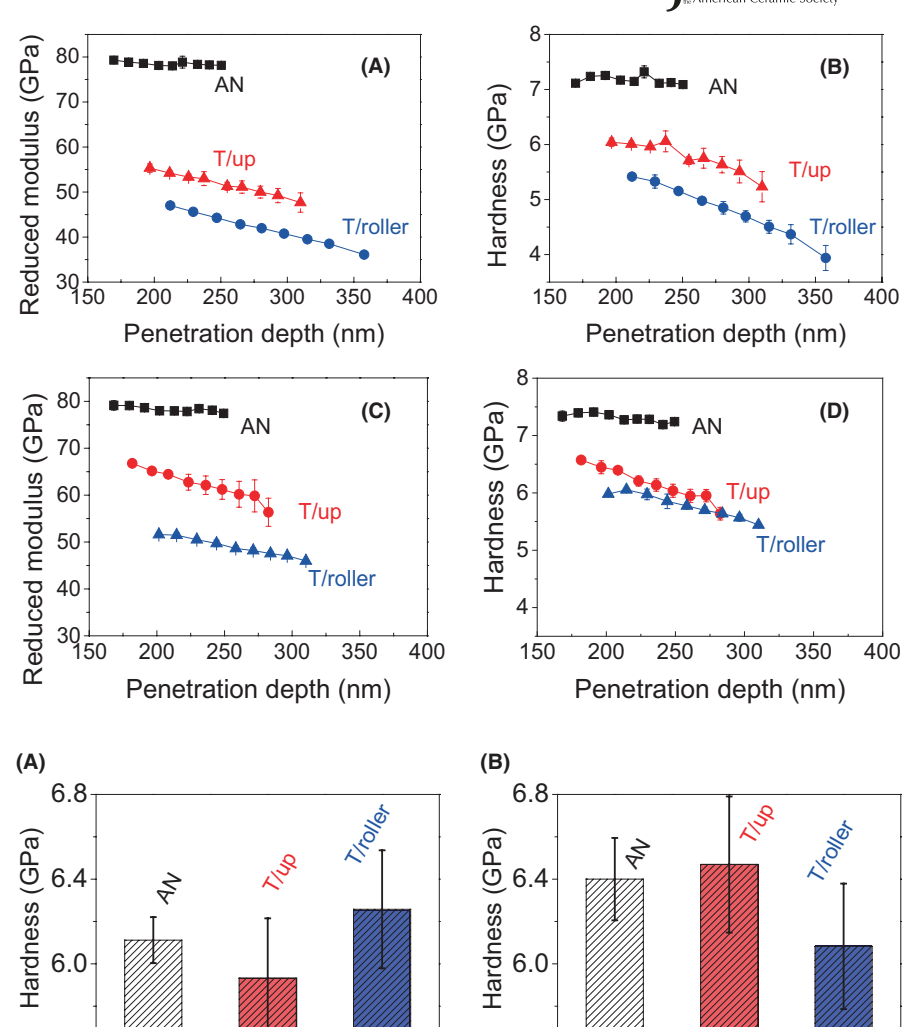


FIGURE 7 Vickers hardness of (A) air-side and (B) tin-side of annealed and tempered glass

the glass surface (Figure 7), although it greatly influences the mechanical responses of the glass surface to the nano-scale indentation (Figures 4 and 5).

5.6

Air side

# 3.4 | Changes in wear behavior of SLS surface upon thermal tempering

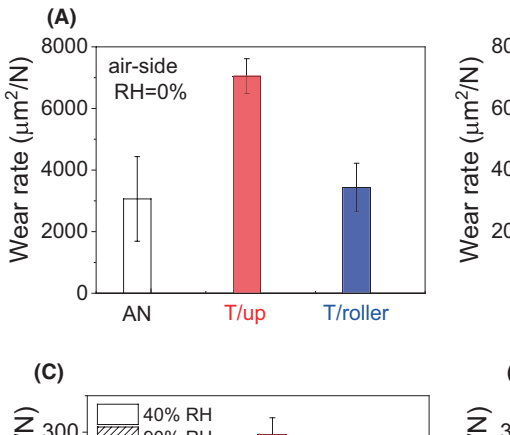
In practical applications, SLS glass panels are subjected to not just normal indentation with an extremely high load but also tangential shear at a light load which is far below the hardness or yield strength of the glass. The friction during the tangential shear can generate mechanical wear (abrasion) in dry condition and mechanochemical (also called tribochemical) wear in humid air. <sup>19-29</sup> Thus, such wear processes can affect the SLS glass panel performance. The wear rates of air-side and tin-side of the annealed and tempered glass were measured at a nominal Hertzian contact pressure of ~380 MPa in dry (0% RH) and humid (40% and 90% RH) conditions and are plotted in Figure 8A,B. In dry condition, the T/up surface of the air-side exhibits a high wear rate (Figure 8A). This

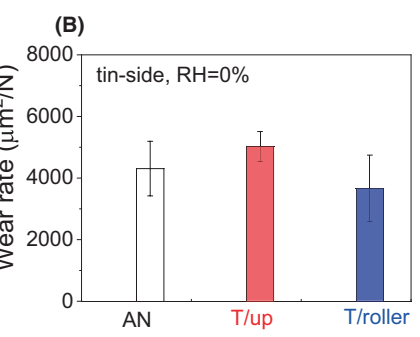
wear (abrasion) rate is greatly affected by the adhesion of wear debris to the counter surface (Figure S3), because it will significantly increase the effective contact pressure at local asperities. Note that it is practically impossible to control the wear debris adhesion during mechanical abrasion and chipping processes because debris are produced stochastically with random shapes.<sup>4</sup>

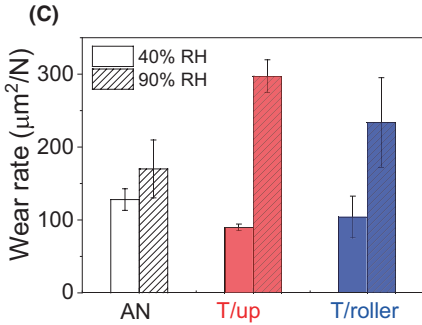
Tin side

5.6

In humid conditions, water adsorbs on the glass surface<sup>50</sup> and those adsorbed water molecules are involved mechanochemical reactions<sup>26,27</sup>; thus, the wear rate decreases significantly compared to the dry condition.<sup>19-29</sup> The wear rates of both annealed and tempered glass surfaces in humid air (Figure 8C,D) are less than 5% of those in dry condition (Figure 8A,B). The counter ball surface is also much smoother after the wear test in humid air (Figure S3). The mechanochemical wear products of the SLS surface adhere to the ball surface in 40% RH, while they are pushed out of the wear track in 90% RH. Thus, it is difficult to compare the effective contact pressure in the wear track in these two different RH conditions although the applied load to the ball is the same (0.2 N).







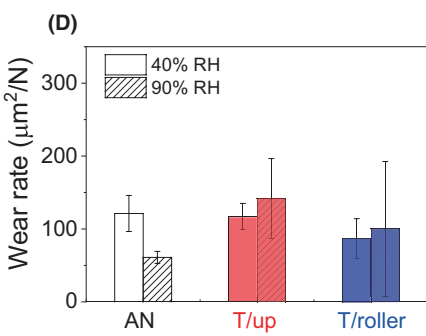


**FIGURE 8** Wear rate of (A) air-side and (B) tin-side of annealed and tempered glass surfaces when tested in dry air. The wear rate of (C) air-side and (D) tin-side of annealed and tempered glass when tested in humid air (40% RH and 90% RH). The error bar is the standard deviation of N = 8 measurements

For the tempered air-side surface, the wear depth (Figure S4A) and volume (Figure 8C) drastically increase upon increasing RH from 40% to 90% RH, while the wear depth and volume at 40% and 90% RH are comparable for the annealed glass. The standard deviation (SD) of the wear depth and volume at 90% RH are larger for the T/roller surface compared to the AN surface, which is consistent with the previous study. The SD of the T/up surface appears to be smaller than that of the T/roller surface, which could be putatively attributed to the fact that the T/up surface is not physically touched during the tempering process, while the T/roller surface makes frequent contacts with the conveyer belt.

For the tin-side, the annealed surface shows a slight decrease in wear depth (Figure S4B) and volume (Figure 8D) upon increasing RH from 40% to 90%; in contrast, the tempered surfaces show no change or a slight increase as RH increases from 40% to 90%. Both T/up and T/down surfaces exhibit significantly larger SD at 90% RH, compared to the AN surface. Although the main cause for such large increase in SD could not be identified in this study, it is still possible to speculate possible reasons. The presence of a small amount of tin can alter the physical properties of SLS glass.<sup>51</sup> Due to a fast cooling via forced air blow, the tempered glass surface may have a higher fictive temperature and thus a larger free volume than the annealed surface.<sup>52</sup> It is also possible that the distribution of the bond parameters of the glass network might be broader in the tempered glass surface due to insufficient time for relaxation during fast cooling, causing local variations in the stress state. These may be responsible, at least partially, for the larger SD of mechanochemical wear depth and volume in high humid conditions. These subtle differences in local structures may not affect the mechanical scratch in dry condition because the stochastic

nature of abrasion is already severe; but they may be manifested as an increase in SD during the mechanochemical process in high humidity condition because such reactions are very sensitive to local strains in chemical bonds. <sup>53,54,55,56</sup> Similar observations were reported for ion-exchanged aluminosilicate glass <sup>21,57</sup> and metals and alloys as well. <sup>58–60</sup>

# 4 | CONCLUSION

The effects of thermal tempering on chemical and mechanical properties of the air- and tin-sides of a SLS float glass were differentiated depending on whether the surface was facing the sliding roller (down) side or the air (upper) side during the tempering process. Before and after tempering, the differences in surface composition measured with XPS, and network structure probed with SR-IR, and micro-hardness evaluated with Vickers indentation were subtle, but there were clearly discernable differences in nanomechanical indentation behaviors and mechanochemical wear behaviors. Those differences are believed to be caused by differences in internal stress gradient due to differences in thermal (cooling rate) and physical contact histories of the roller and air sides during the tempering process as well the chemical composition (absence or presence of tin) in the glass surface.

### **ACKNOWLEDGEMENTS**

This work was supported by the National Science Foundation (Grant No. DMR-2011410) and the National Natural Science Foundation of China (Grant No. 51605401). YTL was supported by Corning, Inc. during the period of this work. The authors also acknowledged Dr. Paul Duffer for arranging



the glass samples for this study, Mr. Rick Wright (Oldcastle Building Envelope) for thermal tempering, and Mr. Paul Bush (Vitro Architectural Glass) for securing a fund to support CQ for the summer undergraduate research.

#### ORCID

Hongtu He https://orcid.org/0000-0002-0734-9729
Hongshen Liu https://orcid.org/0000-0002-2936-1841
Jiaxin Yu https://orcid.org/0000-0003-3578-5760
Seong H. Kim https://orcid.org/0000-0002-8575-7269

#### REFERENCES

- 1. Guldiren D, Erdem İ, Aydin S. Influence of silver and potassium ion exchange on physical and mechanical properties of soda lime glass. J Non-Cryst Solids. 2016;441:1–9.
- Burrows K, Fthenakis V. Glass needs for a growing photovoltaics industry. Sol Energy Mater Sol Cells. 2015;132:455–9.
- Buruga K, Kalathi JT. Performance of halloysite nanotube/poly (styrene-co-methylmethacrylate) nanocomposite coatings for the protection of soda-lime glass. J Alloys Comp. 2019;774:370–7.
- 4. Schneider J, Schula S, Weinhold WP. Characterisation of the scratch resistance of annealed and tempered architectural glass. Thin Solid Films. 2012;520:4190–8.
- Fang Y, Arya F. Evacuated glazing with tempered glass. Sol Energy. 2019;183:240–7.
- Humood M, Beheshti A, Meyer JL, Polycarpoua AA. Normal impact of sand particles with solar panel glass surfaces. Tribol Int. 2016:102:237

  –48.
- Belkhir N, Aliouane T, Bouzid D. Correlation between contact surface and friction during the optical glass polishing. Appl Sur Sci. 2014;288:208–14.
- 8. Varner JR, Oel HJ. Surface defects: their origin, characterization and effects on strength. J Non-Cryst Solids. 1975;19:321–33.
- 9. Freiman SW, Wiederhorn SM, Mecholsky JJ Jr. Environmentally enhanced fracture of glass: a historical perspective. J Am Ceram Soc. 2009;92:1371–82.
- Yoshida S, Sanglebœuf JC, Rouxel T. Quantitative evaluation of indentation-induced densification in glass. J Mater Res. 2005;20(12):3404–12.
- Niu Y, Han K, Guin JP. Locally enhanced dissolution rate as a probe for nanocontact-induced densification in oxide glasses. Langmuir. 2012;28:10733–40.
- 12. Januchta K, Smedskjaer MM. Indentation deformation in oxide glasses: quantification, structural changes, and relation to cracking. J Non-Cryst Solids X. 2019;1:100007.
- 13. Yoshida S, Sawasato H, Sugawara T, Miura Y, Matsuoka J. Effects of indenter geometry on indentation-induced densification of soda-lime glass. J Mate Res. 2010;25(11):2203–21.
- Dey A, Chakraborty R, Mukhopadhyay AK. Nanoindentation of soda lime-silica glass: effect of loading rate. Int J Appl Glass Sci. 2011;2(2):144–55.
- 15. Sellappan P, Rouxel T, Celarie F, Becker E, Houizot P, Conradt R. Composition dependence of indentation deformation and indentation cracking in glass. Acta Mater. 2013;61(16):5949–65.
- Li X, Jiang L, Li J, Mohagheghian I, Dear JP, Li L, et al. Elasticplastic deformation in ion-exchanged aluminosilicate glass by loading rate dependent nanoindentation. J Non-Cryst Solids. 2018;491:79–88.

- Sheth N, Hahn SH, Ngo D, Howzena A, Bermejoy R, van Duin ACT, et al. Influence of acid leaching surface treatment on indentation cracking of soda lime silicate glass. J Non-Cryst Solids. 2020;543:120144.
- Le Houérou V, Sangleboeuf JC, Dériano S. Surface damage of soda-lime-silica glasses: indentation scratch behavior. J Non-Cryst Solids. 2003;316(1):54–63.
- Bradley LC, Dilworth ZR, Barnette AL, Hsiao E, Barthel AJ, Pantano CG, et al. Hydronium ions in soda-lime silicate glass surfaces. J Am Ceram Soc. 2013;96:458–63.
- He H, Qian L, Pantano CG, Kim SH. Mechanochemical wear of soda lime silica glass in humid environments. J Am Ceram Soc. 2014;97(7):2061–8.
- Surdyka ND, Pantano CG, Kim SH. Environmental effects on initiation and propagation of surface defects on silicate glasses: scratch and fracture toughness study. Appl Phys A. 2014;116:519–28.
- He H, Luo J, Qian L, Pantano CG, Kim SH. Thermal Poling of soda-lime silica glass with nonblocking electrodes-Part 2: effects on mechanical and mechanochemical properties. J Am Ceram Soc. 2016;99:1231–8.
- Luo J, Huynh H, Pantano CG, Kim SH. Hydrothermal reactions of soda lime silica glass-revealing subsurface damage and alteration of mechanical properties and chemical structure of glass surfaces. J Non-Cryst Solids. 2016;452:93–101.
- Luo J, Banerjee J, Pantano CG, Kim SH. Vibrational sum frequency generation spectroscopy study of hydrous species in soda lime silica float glass. Langmuir. 2016;32:6035–45.
- He H, Kim SH, Qian L. Effects of contact pressure, counter-surface and humidity on wear of soda-lime-silica glass at nanoscale. Tribol Int. 2016:94:675–81.
- Hahn SH, Liu H, Kim SH, van Duin ACT. Atomistic understanding of surface wear process of sodium silicate glass in dry versus humid environments. J Am Ceram Soc. 2020;103(5):3060–9.
- Yeon J, van Duin ACT, Kim SH. Effects of water on tribochemical wear of silicon oxide interface: molecular dynamics (MD) study with reactive force field (ReaxFF). Langmuir. 2012;32(4):1018–26.
- He H, Xiao T, Qiao Q, Yu J, Zhang Y. Contrasting roles of speed on wear of soda lime silica glass in dry and humid air. J Non-Cryst Solids. 2018;502:236–43.
- He H, Qian L, Pantano CG, Kim SH. Effects of humidity and counter-surface on tribochemical wear of soda-lime-silica glass. Wear. 2015;342:100–6.
- Humood M, Beheshti A, Polycarpou AA. Surface reliability of annealed and tempered solar protective glasses: Indentation and scratch behavior. Sol Energy. 2017;142:13–25.
- 31. Sheth N, Howzen A, Campbell A, Spengler S, Liu H, Pantano CG, et al. Effects of tempering and heat strengthening on hardness, indentation fracture resistance, and wear of soda lime float glass. Int J Appl Glass Sci. 2019;10:431–40.
- Stefan K, Karlsson R, Wondraczek L. Strengthening of oxide glasses. In: Richet P, editor. Encyclopedia for Glass Science, Technology, History and Culture. Hoboken, NJ: John Wiley & Sons Inc.; 2020.
- Novikov VI, Rassada AB. Refinement of Geodetic measurements in construction and operation of float-glass lines with a continuous production cycle. Glass Ceram. 2005;62:202–5.
- Dugnani R, Zednik RJ, Verghese P. Analytical model of dynamic crack evolution in tempered and strengthened glass plates. Int J Fract. 2014;190:75–86.

- Banerjee J, Kim SH, Pantano CG. Elemental areal density calculation and oxygen speciation for flat glass surfaces using x-ray photoelectron spectroscopy. J Non-Cryst Solids. 2016;450:185–93.
- Banerjee J, Bojan V, Pantano CG, Kim SH. Effect of heat treatment on the surface chemical structure of glass: oxygen speciation from in situ XPS analysis. J Am Ceram Soc. 2018;101(2):644–56.
- Pharr G, Oliver W. Measurement of thin film mechanical properties using nanoindentation. MRS Bull. 1992;17(7):28–33.
- 38. Wang X, Kim SH, Chen C, Chen L, He H, Qian L. Humidity dependence of tribochemical wear of monocrystalline silicon. ACS Appl Mater Inter, 2015;7:14785–92.
- Sekine T, Suzuki T, Yamamoto K. Inward migration of glassmodifier cations during heat treatment under an N<sub>2</sub> atmosphere. J Am Ceram Soc. 2015;98(5):1464–70.
- Luo J, Zhou Y, Milner ST, Pantano CG, Kim SH. Molecular dynamics study of correlations between IR peak position and bond parameters of silica and silicate glasses: effects of temperature and stress. J Am Ceram Soc. 2018;101:178–88.
- Liu H, Hahn SH, Ren M, Thiruvillamalai M, Gross TM, Du J, et al. Searching for correlations between vibrational spectral features and structural parameters of silicate glass network. J Am Ceram Soc. 2020;103:3575–89.
- Amma S, Luo J, Pantano CG, Kim SH. Specular reflectance (SR) and attenuated total reflectance (ATR) infrared (IR) spectroscopy of transparent flat glass surfaces: a case study for soda lime float glass. J Non-Cryst Solids. 2015;428:189–96.
- Oliver WC, Pharr GM. Measurement of hardness and elastic modulus by instrumented indentation: advances in understanding and refinements to methodology. J Mater Res. 2004;19(1):3–20.
- Tsui TY, Oliver WC, Pharr GM. Influences of stress on the measurement of mechanical properties using nanoindentation: Part I. Experimental studies in an aluminum alloy. J Mater Res. 1996;11(3):752–9.
- Kese KO, Li ZC, Bergman B. Influence of residual stress on elastic modulus and hardness of soda-lime glass measured by nanoindentation. J Mater Res. 2004;19(10):3109–19.
- 46. Meng QN, Wen M, Hu CQ, Wang SM, Zhang K, Lian JS, et al. Influence of the residual stress on the nanoindentation-evaluated hardness for zirconium nitride films. Sur Coat Tech. 2012;206;3250–7.
- Tadjiev DR, Hand RJ. Surface hydration and nanoindentation of silicate glasses. J Non-Cryst Solids. 2010;356(2):102–8.
- 48. Tadjiev DR, Hand RJ, Zeng P. Comparison of glass hydration layer thickness measured by transmission electron microscopy and nanoindentation. Mater Lett. 2010;64(9):1041–4.
- 49. Pharr GM. Measurement of mechanical properties by ultra-low load indentation. Mater Sci Eng A. 1998;253:151–9.
- Lin Y, Smith NJ, Banerjee J, Agnello G, Manley RG, Walczak WJ, et al. Water adsorption on silica and calcium-boroaluminosilicate

- glass surfaces-thickness and hydrogen bonding of water layer. J Am Ceram Soc. 2021;104(3):1568–80.
- Krohn MH, Hellmann JR, Mahieu B, Pantano CG. Effect of tinoxide on the physical properties of soda-lime-silica glass. J Non-Cryst Solids. 2005;351(6–7):455–65.
- Amma S, Luo J, Kim SH, Pantano CG. Effects of fictive temperature on the leaching of soda lime silica glass surfaces. J Am Ceram Soc. 2017;100(4):1424–31.
- Rimsza JM, Yeon J, van Duin ACT, Du J. Water interactions with nanoporous silica: comparison of ReaxFF and ab Initio based molecular dynamics simulations. J Phys Chem C. 2016;120(43):24803–16.
- Zhu T, Li J, Lin X, Yip S. Stress-dependent molecular pathways of silica-water reaction. J Mech Phys Solids. 2005;53(7):1597–623.
- 55. Gao J, Xiao C, Feng C, Wu L, Yu B, Qian L, et al. Oxidation-induced changes of mechanochemical reactions at GaAs-SiO<sub>2</sub> interface: the competitive roles of water adsorption, mechanical property, and oxidized structure. Appl Sur Sci. 2021;548:149205.
- Wu T, Temizer İ, Wriggers P. Multiscale hydro-thermo-chemomechanical coupling: application to alkali–silica reaction. Comp Mater Sci. 2014;84:381–95.
- Luo J, Grisales W, Rabii M, Pantano CG, Kim SH. Differences in surface failure modes of soda lime silica glass under normal indentation versus tangential shear: a comparative study on Na<sup>+</sup>/K<sup>+</sup>-ion exchange effects. J Am Ceram Soc. 2018;102:1665–76.
- Ryu JJ, Shrotriya P. Mechanical load assisted dissolution response of biomedical cobalt–chromium and titanium metallic alloys: influence of in-plane stress and chemical environment. Wear. 2015;332–333:662–8.
- Ryu JJ, Chua BH, Shrotriya P, Ferraro MM. Influence of in-plane stress state on sliding contact fatigue damage of metallic surfaces. Tribol Int. 2017;116:113–9.
- Mitchell A, Shrotriya P. Onset of nanoscale wear of metallic implant materials: influence of surface residual stresses and contact loads. Wear. 2007;263(7–12):1117–23.

### SUPPORTING INFORMATION

Additional supporting information may be found online in the Supporting Information section.

**How to cite this article:** He H, Liu H, Lin Y-T, Qu C, Yu J, Kim SH. Differences in indentation and wear behaviors between the two sides of thermally tempered soda lime silica glass. *J Am Ceram Soc.* 2021;00:1–10. https://doi.org/10.1111/jace.17872